Journal of Statistical Physics, Vol. 107, Nos. 1/2, April 2002 (© 2002)

Domain Motion in Confined Liquid Crystals

Colin Denniston,[1] Géza Tóth,[2, 3] and J. M. Yeomans[2]

Received February 16, 2001; accepted June 17, 2001

We extend a lattice Boltzmann algorithm of liquid crystal hydrodynamics to include an applied electric field. The approach solves the equations of motion written in terms of a tensor order parameter. Back-flow effects and the hydrodynamics of topological defects are included. We investigate some of the dynamics relevant to liquid crystal devices; in particular defect-mediated motion of domain walls relevant to the nucleation of states useful in pi-cells. An anisotropy in the domain wall velocity is seen because defects of different topology couple differently to the flow field.

KEY WORDS: Lattice Boltzmann; liquid crystals; complex fluids.

1. INTRODUCTION

The coupling of the optic and electric response of liquid crystals has lead to their wide application in display devices in recent years. Liquid crystalline materials are often made up of long, thin, rod-like molecules.[1] This anisotropy is what leads to their useful optic properties. The molecular geometry and interactions can lead to a wide range of equilibrium phases. In this paper we are concerned with the nematic phase where the molecules tend to align along a preferred direction, referred to as the director, giving long-range orientational order. The propensity to order, as well as the direction along which the system orders are conveniently described by a tensor order parameter $\mathbf{Q}$.[1]

An important feature of the nematic phase is the possibility of topological defects. These are director configurations that cannot relax to the

[1] Department of Physics and Astronomy, The Johns Hopkins University, Baltimore, Maryland 21218.

[2] Department of Physics, Theoretical Physics, University of Oxford, 1 Keble Road, Oxford OX1 3NP.

[3] To whom correspondence should be addressed; e-mail: toth@physics.ox.ac.uk

0022-4715/02/0400-0187/0 © 2002 Plenum Publishing Corporation

nematic ground state by a continuous rotation of the molecules. Examples of such defects that we will consider are shown in Fig. 2b. In addition, although widely recognized as an important factor in device performance, the flow of the liquid crystal in response to changes in the orientation of the molecules is both difficult to measure experimentally and to incorporate into a simulation of the device.

Liquid crystal hydrodynamics are typically described by the Ericksen–Leslie–Parodi equations of motion.[1] However these are restricted to an order parameter field of constant magnitude and do not include the hydrodynamics of topological defects. Here we consider the Beris–Edwards formulation of liquid crystal hydrodynamics.[2] This allows for variations in the magnitude of the nematic order parameter and correctly models both defect dynamics and the coupling between the velocity field and the motion of the order parameter.

The Beris–Edwards equations are complex and previous numerical work to explore different flow regimes is very limited. In ref. 3 these equations were used but the problem was simplified by imposing a velocity field and ignoring back-flow (back-flow refers to the effect of the order parameter dynamics on the velocity field). In ref. 4 an Euler solution of a somewhat simpler version of the Beris–Edwards model was used to study the effect of hydrodynamics on phase ordering in liquid crystals. However it has recently been shown that the Beris–Edwards equations can be solved successfully using a lattice Boltzmann algorithm.[5]

In this paper we will extend the lattice Boltzmann approach described in ref. 5 to include the electric field terms necessary for a description of electro-optic device physics. The model is also generalized to include the three elastic constant formula for the deformation free energy of the liquid crystal. The equations of motion are presented in Section II and an outline of the numerical algorithm in Section 3.

We then apply the algorithm to some examples of interest in device physics.[6] The nematic liquid crystal is confined between two plates a few μm apart. The director configuration on the plates is fixed. When an electric field is switched on, the molecules align parallel or perpendicular to the field depending on the sign of the anisotropy of the dielectric constant. After switching off the field, long-range elastic interactions ensure that the molecules reorient themselves in the direction preferred by the surfaces. The device can be used as a display because different liquid crystal orientations have different optical properties.

Switching between different director orientations can take place homogeneously throughout the bulk of the device or it may proceed through domain growth involving the motion of domain walls, together with associated defects.[7] The operational state of a device such as a pi-cell

may be topologically distinct from its state at zero voltage. Before the device can be used, the operational state must be nucleated and must grow to fill the display. It is important to examine how this depends on different parameters of the liquid crystal material. In particular liquid crystals are complex fluids and the speed of domain motion will depend on their hydrodynamic properties.

In Section 4 we examine the global stability of two topologically distinct states as a function of the applied voltage and the tilt angle at the plates. In Section 5 we discuss the relevance of defect motion to domain growth between the two states and show that hydrodynamic coupling significantly changes the defect velocities.

2. THE HYDRODYNAMIC EQUATIONS OF MOTION

We summarize the formulation of liquid crystal hydrodynamics described by Beris and Edwards[2] and extended to include electric fields. The continuum equations of motion are written in terms of a tensor order parameter $\mathbf{Q}$ which is related to the direction of individual molecules $\vec{m}$ by $Q_{\alpha\beta} = \langle m_\alpha m_\beta - \frac{1}{3}\delta_{\alpha\beta} \rangle$ where the angular brackets denote a coarse-grained average. (Greek indices will be used to represent Cartesian components of vectors and tensors and the usual summation over repeated indices will be assumed.) $\mathbf{Q}$ is a traceless symmetric tensor. Its largest eigenvalue, $\frac{2}{3}q$, $0 < q < 1$, describes the magnitude of the order.

We first write down a Landau free energy which describes the equilibrium properties of the liquid crystal. This appears in the equation of motion of the order parameter, which includes a Cahn–Hilliard-like term through which the system evolves towards thermodynamic equilibrium.

Free Energy: The equilibrium properties of a nematic liquid crystal can be described by the Landau–de Gennes free energy[1, 8]

$$\mathscr{F} = \int_V dV \{ f_{\text{bulk}} + f_{\text{elastic}} + f_{\text{field}} \} + \int_S dS \{ f_{\text{surf}} \} \tag{1}$$

f_{bulk} describes the bulk free energy

$$f_{\text{bulk}} = \frac{A_0}{2}\left(1 - \frac{\gamma}{3}\right) Q_{\alpha\beta}^2 - \frac{A_0\gamma}{3} Q_{\alpha\beta} Q_{\beta\gamma} Q_{\gamma\alpha} + \frac{A_0\gamma}{4} (Q_{\alpha\beta}^2)^2 \tag{2}$$

For $\gamma = 2.7$ there is a first-order transition from the isotropic to the nematic phase. f_{elastic} is the analogue of the Frank elastic free energy density

$$f_{\text{elastic}} = \frac{L_1}{2} (\partial_\alpha Q_{\beta\gamma})^2 + \frac{L_2}{2} (\partial_\alpha Q_{\alpha\gamma})(\partial_\beta Q_{\beta\gamma}) + \frac{L_3}{2} Q_{\alpha\beta} (\partial_\alpha Q_{\gamma\epsilon})(\partial_\beta Q_{\gamma\epsilon}) \tag{3}$$

The dielectric constant is usually measured along and perpendicular to the nematic axis, $\vec{n}$, and is usually assumed to give a relation between the electric displacement $\mathbf{D}$ and field $\mathbf{E}$ of the form

$$\mathbf{D} = \epsilon_\perp \mathbf{E} + (\epsilon_\parallel - \epsilon_\perp)(\vec{n} \cdot \mathbf{E})\, \vec{n} \tag{4}$$

For a uniaxial nematic, this is entirely equivalent to assuming that

$$\epsilon_{\alpha\beta} = \tfrac{2}{3} \epsilon_a Q_{\alpha\beta} + \epsilon_m \delta_{\alpha\beta} \tag{5}$$

where

$$\epsilon_a = \frac{3}{2q} (\epsilon_\parallel - \epsilon_\perp) \tag{6}$$

$$\epsilon_m = \frac{2}{3} \epsilon_\perp + \frac{1}{3} \epsilon_\parallel \tag{7}$$

The electric contribution to the thermodynamic potential f_{field} is

$$f_{\text{field}} = -\frac{1}{4\pi} \int \mathbf{D} \cdot d\mathbf{E} = -\frac{1}{8\pi} \epsilon_m E^2 - \frac{1}{12\pi} \epsilon_a E_\alpha E_\beta Q_{\alpha\beta} \tag{8}$$

At the surfaces of the device we assume a pinning potential

$$f_{\text{surf}} = \tfrac{1}{2} \alpha_S (Q_{\alpha\beta} - Q^0_{\alpha\beta})^2 \tag{9}$$

This corresponds to a director at the surface preferring to lie along the direction of the eigenvector of $\mathbf{Q}^0$ corresponding to the largest eigenvalue $2/3q$.

Equation of Motion of the Nematic Order Parameter: The equation of motion for the nematic order parameter is[2]

$$(\partial_t + \vec{u} \cdot \nabla)\, \mathbf{Q} - \mathbf{S}(\mathbf{W}, \mathbf{Q}) = \Gamma \mathbf{H} \tag{10}$$

where Γ is a collective rotational diffusion constant. The first term on the left-hand side of Eq. (10) is the material derivative describing the usual time dependence of a quantity advected by a fluid with velocity $\vec{u}$. This is generalized by a second term

$$\begin{aligned} \mathbf{S}(\mathbf{W}, \mathbf{Q}) = {} & (\xi \mathbf{\Lambda} + \mathbf{\Omega})(\mathbf{Q} + \mathbf{I}/3) + (\mathbf{Q} + \mathbf{I}/3)(\xi \mathbf{\Lambda} - \mathbf{\Omega}) \\ & - 2\xi (\mathbf{Q} + \mathbf{I}/3)\, \mathrm{Tr}(\mathbf{Q}\mathbf{W}) \end{aligned} \tag{11}$$

where $\mathbf{\Lambda} = (\mathbf{W} + \mathbf{W}^T)/2$ and $\mathbf{\Omega} = (\mathbf{W} - \mathbf{W}^T)/2$ are the symmetric part and the anti-symmetric part respectively of the velocity gradient tensor $W_{\alpha\beta} = \partial_\beta u_\alpha$. $\mathbf{S}(\mathbf{W}, \mathbf{Q})$ appears in the equation of motion because the order parameter distribution can be both rotated and stretched by flow gradients. This is the consequence of the rod-like geometry of the liquid crystal molecules. ξ is a constant which will depend on the molecular details of a given liquid crystal.

The term on the right-hand side of Eq. (10) describes the relaxation of the order parameter towards the minimum of the free energy. The molecular field $\mathbf{H}$ which provides the driving motion is related to the derivative of the free energy by

$$\begin{aligned}\mathbf{H} &= -\frac{\delta \mathscr{F}}{\delta \mathbf{Q}} + (\mathbf{I}/3)\,\mathrm{Tr}\,\frac{\delta \mathscr{F}}{\delta \mathbf{Q}} \\ &= \mathbf{H}_{\text{bulk}} + \mathbf{H}_{\text{elastic}} + \mathbf{H}_{\text{field}} + \mathbf{H}_{\text{surf}}\end{aligned} \tag{12}$$

where

$$\mathbf{H}_{\text{bulk}} = -A_0\left(1 - \frac{\gamma}{3}\right)\mathbf{Q} + A_0\gamma(\mathbf{Q}^2 - (\mathbf{I}/3)\,\mathrm{Tr}\,\mathbf{Q}^2) - A_0\gamma\mathbf{Q}\,\mathrm{Tr}\,\mathbf{Q}^2 \tag{13}$$

$$\begin{aligned}H_{\text{elastic},\,\alpha\beta} = {} & L_1(\partial_\gamma{}^2 Q_{\alpha\beta}) + L_2\left\{\frac{1}{2}(\partial_\alpha\partial_\gamma Q_{\gamma\beta} + \partial_\beta\partial_\gamma Q_{\gamma\alpha}) - \frac{1}{3}\delta_{\alpha\beta}\partial_\gamma\partial_\epsilon Q_{\gamma\epsilon}\right\} \\ & + \frac{1}{2}L_3\left\{\partial_\gamma(Q_{\gamma\epsilon}\partial_\epsilon Q_{\alpha\beta}) - (\partial_\alpha Q_{\gamma\epsilon})(\partial_\beta Q_{\gamma\epsilon}) + \frac{1}{3}\delta_{\alpha\beta}(\partial_\eta Q_{\gamma\epsilon})^2\right\}\end{aligned} \tag{14}$$

$$H_{\text{field},\,\alpha\beta} = \frac{\epsilon_a}{12\pi}\left(E_\alpha E_\beta - \frac{\delta_{\alpha\beta}}{3}E_\gamma{}^2\right) \tag{15}$$

$$\mathbf{H}_{\text{surf}} = -\alpha_S(\mathbf{Q} - \mathbf{Q}^0) \tag{16}$$

and $\delta_{\alpha\beta}$ is the Kronecker delta. For (14) $\partial_z = 0$ is assumed, and the symmetry and tracelessness of $\mathbf{Q}$ is also exploited for simplification.

When computing the functional derivative in (12) surface terms arise from the integration by parts. For reference, these are

$$\begin{aligned}\delta\mathscr{F}_d^{\text{surf}} = \int_{\partial V} ds\,\delta Q_{\alpha\beta}\{ & L_1\sigma_\gamma(\partial_\gamma Q_{\alpha\beta}) + \tfrac{1}{2}L_2[\sigma_\alpha(\partial_\gamma Q_{\gamma\beta}) + \sigma_\beta(\partial_\gamma Q_{\gamma\alpha})] \\ & + L_3\sigma_\gamma Q_{\gamma\epsilon}(\partial_\epsilon Q_{\alpha\beta})\}\end{aligned} \tag{17}$$

where $\boldsymbol{\sigma}$ is the surface (unit) normal.

Continuity and Navier–Stokes Equations: The fluid momentum obeys the continuity

$$\partial_t \rho + \partial_\alpha \rho u_\alpha = 0 \tag{18}$$

and the Navier–Stokes equation

$$\rho \partial_t u_\alpha + \rho u_\beta \partial_\beta u_\alpha = \partial_\beta \tau_{\alpha\beta} + \partial_\beta \sigma_{\alpha\beta} + \frac{\rho \tau_f}{3} \partial_\beta ((\delta_{\alpha\beta} - 3\partial_\rho P_0)\, \partial_\gamma u_\gamma + \partial_\alpha u_\beta + \partial_\beta u_\alpha) \tag{19}$$

where ρ is the fluid density and τ_f is related to the viscosity. The form of this equation is not dissimilar to that for a simple fluid. However the details of the stress tensor reflect the additional complications of liquid crystal hydrodynamics. There is a symmetric contribution

$$\sigma_{\alpha\beta} = -P_0 \delta_{\alpha\beta} - \xi H_{\alpha\gamma} \left(Q_{\gamma\beta} + \frac{1}{3} \delta_{\gamma\beta} \right) - \xi \left(Q_{\alpha\gamma} + \frac{1}{3} \delta_{\alpha\gamma} \right) H_{\gamma\beta} + 2\xi \left(Q_{\alpha\beta} + \frac{1}{3} \delta_{\alpha\beta} \right) Q_{\gamma\epsilon} H_{\gamma\epsilon} - \partial_\beta Q_{\gamma\nu} \frac{\delta \mathscr{F}}{\delta \partial_\alpha Q_{\gamma\nu}} + \sigma_{M,\alpha\beta} \tag{20}$$

and an antisymmetric contribution

$$\tau_{\alpha\beta} = Q_{\alpha\gamma} H_{\gamma\beta} - H_{\alpha\gamma} Q_{\gamma\beta} \tag{21}$$

The background pressure P_0 is taken simply to be

$$P_0 = \rho T \tag{22}$$

and is found to be a constant in our simulations to a very good approximation. The Maxwell stress tensor $\sigma_{M,\alpha\beta}$[9] describes the stress due to the external electric field

$$\sigma_{M,\alpha\beta} = \frac{1}{8\pi} (D_\alpha E_\beta + E_\alpha D_\beta - D_\gamma E_\gamma \delta_{\alpha\beta}) \tag{23}$$

3. A LATTICE BOLTZMANN ALGORITHM FOR LIQUID CRYSTAL HYDRODYNAMICS

We now describe a lattice Boltzmann algorithm which solves the hydrodynamic equations of motion of a liquid crystal (10), (18), and (19).

Lattice Boltzmann algorithms are defined in terms of a set of continuous variables, usefully termed partial distribution functions, which move on a lattice in discrete space and time.[10]

The simplest lattice Boltzmann algorithm, which solves the Navier–Stokes equations of a simple fluid, is defined in terms of a single set of partial distribution functions which sum on each site to give the density. For liquid crystal hydrodynamics this must be supplemented by a second set, which are tensor variables, and which are related to the tensor order parameter $\mathbf{Q}$.[5]

We define two distribution functions, the scalars $f_i(\vec{x})$ and the symmetric traceless tensors $\mathbf{G}_i(\vec{x})$ on each lattice site $\vec{x}$. Each f_i, $\mathbf{G}_i$ is associated with a lattice vector $\vec{e}_i$. We choose a nine-velocity model on a square lattice with velocity vectors $\vec{e}_i = (\pm 1, 0), (0, \pm 1), (\pm 1, \pm 1), (0, 0)$. Physical variables are defined as moments of the distribution function

$$\rho = \sum_i f_i, \qquad \rho u_\alpha = \sum_i f_i e_{i\alpha}, \qquad \mathbf{Q} = \sum_i \mathbf{G}_i \tag{24}$$

The distribution functions evolve in a time step Δt according to

$$f_i(\vec{x} + \vec{e}_i\,\Delta t, t + \Delta t) - f_i(\vec{x}, t) = \frac{\Delta t}{2}\left[\mathscr{C}_{fi}(\vec{x}, t, \{f_i\}) + \mathscr{C}_{fi}(\vec{x} + \vec{e}_i\,\Delta t, t + \Delta t, \{f_i^*\})\right] \tag{25}$$

$$\mathbf{G}_i(\vec{x} + \vec{e}_i\,\Delta t, t + \Delta t) - \mathbf{G}_i(\vec{x}, t) = \frac{\Delta t}{2}\left[\mathscr{C}_{\mathbf{G}i}(\vec{x}, t, \{\mathbf{G}_i\}) + \mathscr{C}_{\mathbf{G}i}(\vec{x} + \vec{e}_i\,\Delta t, t + \Delta t, \{\mathbf{G}_i^*\})\right] \tag{26}$$

This represents free streaming with velocity $\vec{e}_i$ and a collision step which allows the distribution to relax towards equilibrium. f_i^* and $\mathbf{G}_i^*$ are first order approximations to $f_i(\vec{x} + \vec{e}_i\,\Delta t, t + \Delta t)$ and $\mathbf{G}_i(\vec{x} + \vec{e}_i\,\Delta t, t + \Delta t)$ respectively. Discretizing in this way, which is similar to a predictor-corrector scheme, means that lattice viscosity terms are eliminated. In a lattice Boltzmann algorithm for a simple fluid these terms can be added to the physical viscosity term. Here this is not the case: the lattice viscosity gives an additional, spurious term in the equations of motion. An additional advantage of the predictor-corrector approach is that the stability of the lattice Boltzmann algorithm is improved. The collision operators are taken to have the form of a single relaxation time Boltzmann equation,[10] together with a forcing term

$$\mathscr{C}_{fi}(\vec{x}, t, \{f_i\}) = -\frac{1}{\tau_f}(f_i(\vec{x}, t) - f_i^{\mathrm{eq}}(\vec{x}, t, \{f_i\})) + p_i(\vec{x}, t, \{f_i\}) \tag{27}$$

$$\mathscr{C}_{\mathbf{G}i}(\vec{x}, t, \{\mathbf{G}_i\}) = -\frac{1}{\tau_g}(\mathbf{G}_i(\vec{x}, t) - \mathbf{G}_i^{\mathrm{eq}}(\vec{x}, t, \{\mathbf{G}_i\})) + \mathbf{M}_i(\vec{x}, t, \{\mathbf{G}_i\}) \tag{28}$$

The form of the equations of motion and thermodynamic equilibrium follow from the choice of the moments of the equilibrium distributions f_i^{eq} and $\mathbf{G}_i^{\mathrm{eq}}$ and the driving terms p_i and $\mathbf{M}_i$. f_i^{eq} is constrained by

$$\sum_i f_i^{\mathrm{eq}} = \rho, \qquad \sum_i f_i^{\mathrm{eq}} e_{i\alpha} = \rho u_\alpha, \qquad \sum_i f_i^{\mathrm{eq}} e_{i\alpha} e_{i\beta} = -\sigma_{\alpha\beta} + \rho u_\alpha u_\beta \tag{29}$$

where the zeroth and first moments are chosen to impose conservation of mass and momentum. The second moment of f^{eq} controls the symmetric part of the stress tensor, whereas the moments of p_i

$$\sum_i p_i = 0, \qquad \sum_i p_i e_{i\alpha} = \partial_\beta \tau_{\alpha\beta}, \qquad \sum_i p_i e_{i\alpha} e_{i\beta} = 0 \tag{30}$$

impose the antisymmetric part of the stress tensor. For the equilibrium of the order parameter distribution we choose

$$\sum_i \mathbf{G}_i^{\mathrm{eq}} = \mathbf{Q}, \qquad \sum_i \mathbf{G}_i^{\mathrm{eq}} e_{i\alpha} = \mathbf{Q} u_\alpha, \qquad \sum_i \mathbf{G}_i^{\mathrm{eq}} e_{i\alpha} e_{i\beta} = \mathbf{Q} u_\alpha u_\beta \tag{31}$$

This ensures that the order parameter is convected with the flow. Finally the evolution of the order parameter is most conveniently modeled by choosing

$$\sum_i \mathbf{M}_i = \Gamma \mathbf{H}(\mathbf{Q}) + \mathbf{S}(\mathbf{W}, \mathbf{Q}) \equiv \hat{\mathbf{H}}, \qquad \sum_i \mathbf{M}_i e_{i\alpha} = \left(\sum_i \mathbf{M}_i\right) u_\alpha \tag{32}$$

which ensures that the fluid minimizes its free energy at equilibrium.

Conditions (29)–(32) can be satisfied as is usual in lattice Boltzmann schemes by writing the equilibrium distribution functions and forcing terms as polynomial expansions in the velocity[10]

$$\begin{aligned} f_i^{\mathrm{eq}} &= A_s + B_s u_\alpha e_{i\alpha} + C_s u^2 + D_s u_\alpha u_\beta e_{i\alpha} e_{i\beta} + E_{s\alpha\beta} e_{i\alpha} e_{i\beta} \\ \mathbf{G}_i^{\mathrm{eq}} &= \mathbf{J}_s + \mathbf{K}_s u_\alpha e_{i\alpha} + \mathbf{L}_s u^2 + \mathbf{N}_s u_\alpha u_\beta e_{i\alpha} e_{i\beta} \\ p_i &= T_s \partial_\beta \tau_{\alpha\beta} e_{i\alpha} \\ \mathbf{M}_i &= \mathbf{R}_s + \mathbf{S}_s u_\alpha e_{i\alpha} \end{aligned} \tag{33}$$

where $s = \vec{e}_i^{\,2} \in \{0, 1, 2\}$ identifies separate coefficients for different absolute values of the velocities. A suitable choice is

$$
\begin{gathered}
A_2 = -(\sigma_{xx} + \sigma_{yy})/16, \qquad A_1 = 2A_2, \qquad A_0 = \rho - 12A_2 \\
B_2 = \rho/12, \qquad B_1 = 4B_2 \\
C_2 = -\rho/16, \qquad C_1 = -\rho/8, \qquad C_0 = -3\rho/4 \\
D_2 = \rho/8, \qquad D_1 = \rho/2 \\
E_{2xx} = (\sigma_{yy} - \sigma_{xx})/16, \qquad E_{2yy} = -E_{2xx}, \qquad E_{2xy} = E_{2yx} = -\sigma_{xy}/8 \\
E_{1xx} = 4E_{2xx}, \qquad E_{1yy} = 4E_{2yy} \\
\mathbf{J}_0 = \mathbf{Q} \\
\mathbf{K}_2 = \mathbf{Q}/12, \qquad \mathbf{K}_1 = 4\mathbf{K}_2 \\
\mathbf{L}_2 = -\mathbf{Q}/16, \qquad \mathbf{L}_1 = -\mathbf{Q}/8, \qquad \mathbf{L}_0 = -3\mathbf{Q}/4 \\
\mathbf{N}_2 = \mathbf{Q}/8, \qquad \mathbf{N}_1 = \mathbf{Q}/2 \\
T_2 = 1/12, \qquad T_1 = 4T_2 \\
\mathbf{R}_2 = \hat{\mathbf{H}}/9, \qquad \mathbf{R}_1 = \mathbf{R}_0 = \mathbf{R}_2 \\
\mathbf{S}_2 = \hat{\mathbf{H}}/12, \qquad \mathbf{S}_1 = 4\mathbf{S}_2
\end{gathered}
\tag{34}
$$

where any coefficients not listed are zero.

4. H-V PHASE DIAGRAM

We now use the lattice Boltzmann algorithm described in Sections 2 and 3 to investigate a simple liquid crystal device. The device consists of a nematic liquid crystal confined between two planes a distance L_x apart. At the surface $\mathbf{Q}^0$ is chosen to give a surface tilt to the director of $+\theta_p$ at $x = 0$ and $-\theta_p$ at $x = L_x$. At zero applied voltage these conditions result in a global minimum free energy state with a splayed director configuration, or H state as shown in Fig. 1a. At high voltages, typically on order of $6V$, the H state is no longer the global minimum, and a bend configuration (V state) is obtained like the one shown in Fig. 1b. At intermediate voltages, the V state is more relaxed, like the one shown in Fig. 1c.

The V state may remain for some time even at zero voltage as it is metastable. As the H and V states are topologically distinct, the transition from one to the other requires nucleation and the generation of defects. This process is illustrated in Fig. 2.

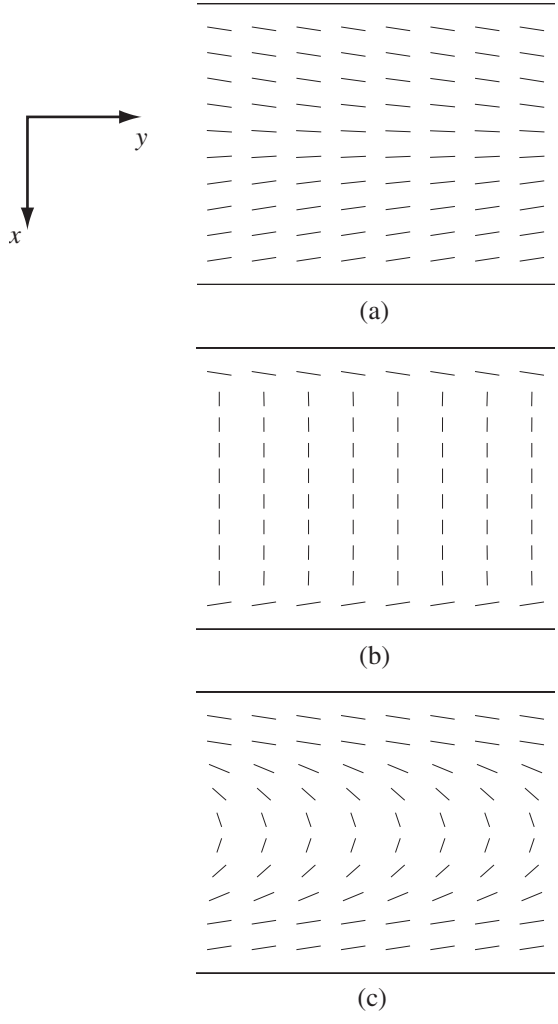

Fig. 1. Alignment of molecules for a tilt angle $+\theta_p$ on the top surface and $-\theta_p$ on the bottom surface. Director configuration when $\theta_p < 45°$ and (a) the field is switched off and the system has had time to relax to its global minimum; (b) the field is switched on the a fairly high voltage $\sim 6V$; and (c) the field is at a low voltage $\sim 2V$ or lower. The system may remain in the metastable state (c) for some time even at zero voltage.

The simulations were performed on a 48×48 grid. We used $L_1 = 0.0440$, $L_2 = 0.0445$, $L_3 = 0.0606$, $\epsilon_a = 41.4$, $\epsilon_m = 9.8$, $A_0 = 1.0$ and $\gamma = 3.0$. By a choice of appropriate length, time and pressure scales these correspond to physical values values $L_1 = 17.4$ pN, $L_2 = 17.6$ pN, $L_3 = 24.2$ pN, $L_x = L_y = 3$ μm which is consistent with the nematic liquid crystal E7

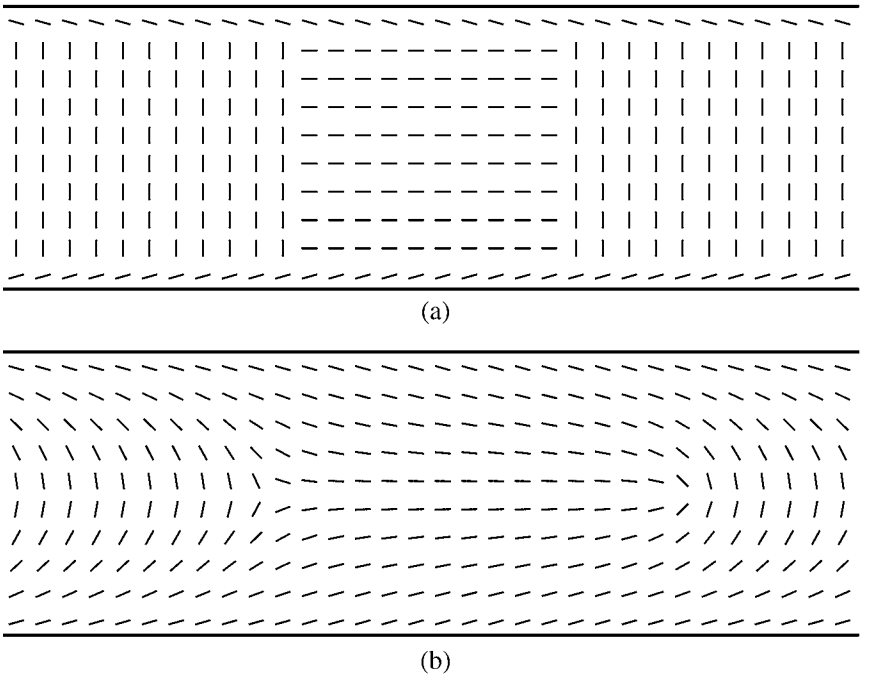

Fig. 2. (a) Initial director configuration used to study domain growth. After the vertical electric field is switched off, a horizontal domain is created in order to nucleate the growth process. (b) Shortly thereafter two defects are formed at the boundary of the horizontal and vertical domains. The left (right) defect has a topological strength $s = -\frac{1}{2}$ ($s = +\frac{1}{2}$). Both the horizontal and the vertical domains are slightly distorted due to the defects and the surface tilt.

(Merck Ltd. UK) at 25°C. Periodic boundary conditions were used in the y-direction and bounce-back in the x-direction.

A phase diagram for the H and V states in the tilt angle/voltage plane is shown in Fig. 3. The system was started in a configuration like that shown Fig. 2. For low fields the H domain has a lower free energy density, thus it grows (crosses). For high enough fields the H domain shrinks (circles). The boundary is defined as the voltage at which the two domains have the same free energy. This diagram compares well with those measured experimentally for a system using E7.[7]

5. DOMAIN GROWTH

Consider the dynamics of the domain growth in the system. Rather than fix parameters to a specific material, we wish to explore how the

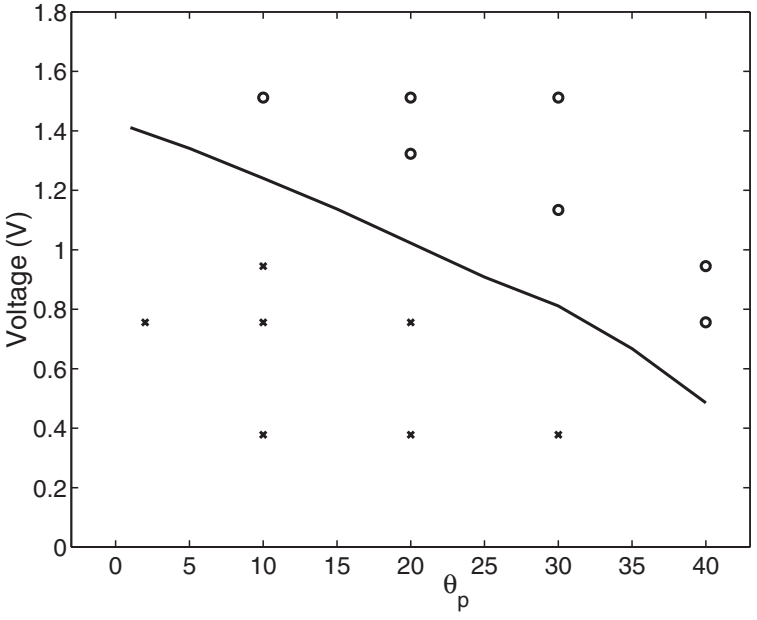

Fig. 3. Phase diagram for the H and V states as a function of tilt angle and voltage. At low fields (crosses) the H domain has a lower free energy density, thus it grows. If the field strong enough (circles), the H domain shrinks. On the line the two domains have equal free energy density.

dynamics are affected by different parameters. In particular, we are interested in how hydrodynamics affects the speed of the domain growth. This is motivated by the observation in ref. 7 that the domain growth was anisotropic and the speculation that this may be due to hydrodynamics. To isolate effects due to different elastic constants, for these simulations we set $L_2 = L_3 = 0.0$, the so-called one-elastic constant approximation.

The initial configuration, depicted in Fig. 2a, is a horizontal (i.e., along the y-direction) domain in an otherwise vertically aligned state. This models a time shortly after the electric field has been switched off when small but macroscopic domains have formed in the device.

Once the simulation commences the director configuration relaxes rapidly to that shown in Fig. 2b. The horizontal and vertical domains are both tilted slightly by the elastic coupling to the surface spins. Then defects are formed at the domain boundaries, which merge to form single defects with strengths $\pm 1/2$ at the centre of each domain wall respectively. Once the two defects have formed the vertical domain begins to grow and the defects move in opposite directions. Our aim is to investigate the effect of

back-flow and surface director tilt on this motion. Most previous work on the dynamics of topological defects has ignored the back-flow.[11–14]

We first investigate the effect of the surface tilt θ_p on the defect speed. The horizontal domain grows because it decreases the free energy of the device. It can be shown[7] that the difference in free energy between the horizontal and vertical domains is proportional to $45° - \theta_p$, where θ_p is the angle of the surface tilt to the y-axis. Thus as θ_p increases, the free energy difference decreases, and the defects move more slowly. At $\theta_p = 45°$ the two domains have the same free energy and the defects stop moving. For $\theta_p > 45°$ the horizontal domain begins to shrink.

A particular advantage of the simulation is that the back-flow can easily be switched off by setting $\sigma_{\alpha\beta} = -P_0\delta_{\alpha\beta}$ and $\tau_{\alpha\beta}$ to zero in (33) and (34). Thus the effect of the back-flow can be unambiguously identified. Since no flow is imposed, this leads to a zero velocity field throughout the whole simulation. The dynamical equation for the system in this case can be obtained from (10) by setting $\vec{u}$ to zero. It corresponds to a simpler model which does not include hydrodynamics.

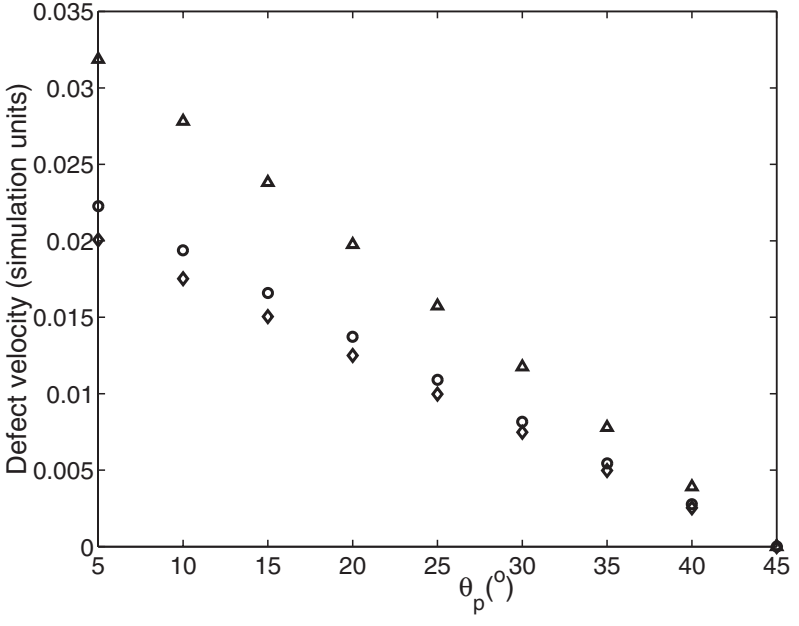

Fig. 4. The velocity of the two defects as the function of surface tilt if back-flow is ignored (diamonds) and included. Notice that if back-flow is not included then the two defects move with the same speed. Hydrodynamics accelerates the $s = +\frac{1}{2}$ defect (triangles) substantially, while it affects less the $s = -\frac{1}{2}$ defect (circles).

Consider first the diamonds in Fig. 4. This corresponds to the case with back-flow switched off. For this case both defects move at the same speed (but in opposite directions). This can be explained by considering a local co-ordinate transformation $x \to -x$ which is equivalent to changing the sign of the off-diagonal elements in $\mathbf{Q}$. Assuming $\vec{u} = 0$, the dynamical equation (10) is invariant under this transformation whereas the two defects in Fig. 2b transform into each other.

The triangles and circles in Fig. 4 show the velocity of the defects when back-flow is included in the model. Now the two defects move with

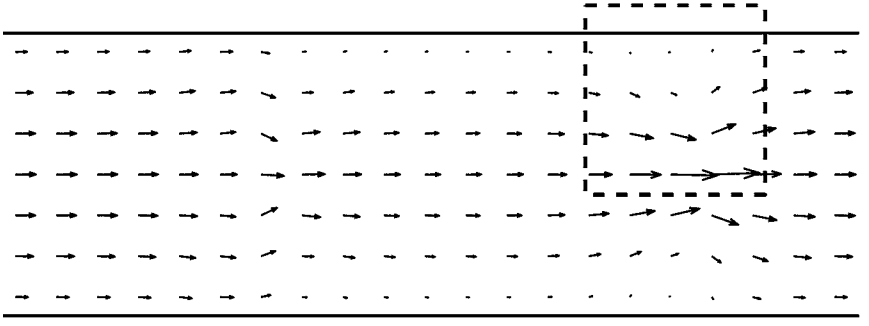

(a)

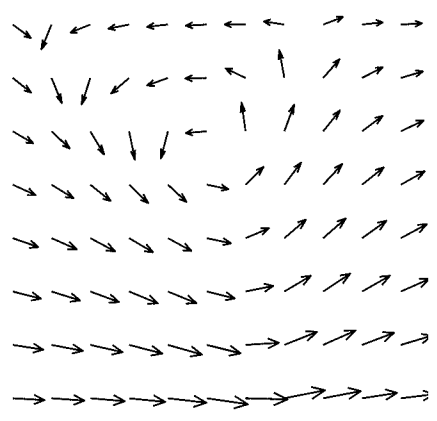

(b)

Fig. 5. (a) Velocity field corresponding to the director configuration shown in Fig. 2b. Notice that there is a strong vortex structure around the $s = +\frac{1}{2}$ defect and at the defect core it points in the direction of defect movement. The flow at the core of the other defect is much weaker. (b) Flow field corresponding to the dashed box. For better visibility the length of the vectors is changed disproportionally.

different speeds since the xy elements of the stress tensors (20) and (21) are not invariant under the $x \to -x$ transformation. Thus the stress fields are different for the two defects. Due to this stress field two different flow fields are formed around the defects (see Fig. 5). The flow is stronger around the $s = +\frac{1}{2}$ defect and it is substantially accelerated. The speed of the $s = -\frac{1}{2}$ defect is affected much less by the flow.

An experimental setup similar to Fig. 2 was considered in ref. 7 where the growth of a circular twist domain in a horizontal environment under the influence of an external field was studied for different surface tilt values. It was found that the domain growth was anisotropic. Although this problem is three-dimensional, a vertical cross section through the growing domain gives a geometry similar to that considered here. It seems extremely plausible, that the essential physics is captured by our model with the anisotropy in growth resulting from the difference in the flow fields corresponding to different defect topologies at the defect boundary. Quantitative mappings between the experiment and the simulation results must be treated with caution because of the different dimensionality. However, in both the simulation and the experiment the difference between the wall speeds was about 40–50%.

The simulations were performed on a 700×48 grid. We used $L_1 = 1.0$, $L_2 = L_3 = 0$, $A_0 = 5.0$, $\gamma = 3.0$, $\Gamma = 0.44$, $\xi = 0.52$ and $\tau_f = 1.0$. The larger L_1 corresponds to increasing the resolution of the lattice in order to perform accurate defect velocity measurements.

6. SUMMARY AND DISCUSSION

In this paper we have described a lattice Boltzmann algorithm to simulate the dynamics of a non-Newtonian fluid, liquid crystals.

In particular we have considered the the presence of an external electric field and the possibility of a general Frank free energy with three elastic constants. In the continuum limit we recover the Beris–Edwards formulation within which the liquid crystal equations of motion are written in terms of a tensor order parameter.[2] The equations are applicable to the isotropic, uniaxial nematic, and biaxial nematic phases. Working within the framework of a variable tensor order parameter it is possible to simulate variations in the magnitude of order and hence the dynamics of topological defects and non-equilibrium phase transitions between different flow regimes.

The algorithm was used to explore states in nematic liquid crystal devices. We find that switching between topologically distinct states is, as expected, strongly inhibited by a free energy barrier between the initial and the final states. In this case the state can only change once a domain of the

final state has been nucleated. Defects form at the moving domain walls and hence this geometry allows an investigation of defect hydrodynamics. We find that a $s = +\frac{1}{2}$ defect is substantially speeded up by back-flow effects. This is relevant to device physics where the speed of switching is an important design variable.

There are many directions for further research opened up by the rich physics inherent in liquid crystal hydrodynamics and the generality of the Beris–Edwards equations. For example, another possible switching pathway would be via the escape of the director into a third dimension. The addition of flexoelectric terms to the equations of motion will allow problems relevant to bistable liquid crystal displays to be addressed. Even cases where the switching is the consequence of back-flow[15] can be modeled. Numerical investigations are vital to address these problems because of the complexity of the equations of motion.

REFERENCES

1. P. G. de Gennes and J. Prost, *The Physics of Liquid Crystals*, 2nd ed. (Clarendon Press, Oxford, 1993).
2. A. N. Beris and B. J. Edwards, *Thermodynamics of Flowing Systems* (Oxford University Press, Oxford, 1994); A. N. Beris, B. J. Edwards, and M. Grmela, *J. Non-Newtonian Fluid Mechanics* **35**:51 (1990).
3. A. D. Rey and T. Tsuji, *Macromol. Theory Simul.* **7**:623 (1998); T. Tsuji and A. Rey, *Phys. Rev. E* **57**:5609 (1998); T. Tsuji and A. Rey, *J. Non-Newtonian Fluid Mech.* **73**:127 (1997).
4. J.-i Fukuda, *Eur. Phys. J. B* **1**:173 (1998).
5. C. Denniston, E. Orlandini, and J. M. Yeomans, *Europhys. Lett.* **52**:481 (2000); C. Denniston, E. Orlandini, and J. M. Yeomans, *Phys. Rev. E*, in press.
6. T. J. Sluckin, *Contemporary Physics* **41**:37 (2000).
7. E. J. Acosta, M. J. Towler, and H. G. Walton, *Liquid Cryst.* **27**:977 (2000).
8. S. A. Pikin, *Structural Transformations in Liquid Crystals* (Gordon & Breach Science Publishers, 1991).
9. L. D. Landau and E. M. Lifshitz, *Electrodynamics of Continuous Media* (Pergamon Press, New York, 1960).
10. S. Chen and G. D. Doolen, *Annual Rev. Fluid Mech.* **30**:329 (1998).
11. C. Denniston, *Phys. Rev. B* **54**:6272 (1996).
12. L. M. Pismen and B. Y. Rubinstein, *Phys. Rev. Lett.* **69**:96 (1992).
13. G. Ryskin and M. Kremenetsky, *Phys. Rev. Lett.* **67**, 1574 (1991).
14. Q. Jiang, J. E. Maclennan, and N. A. Clark, *Phys. Rev. E* **53**:6074–6079 (1996).
15. I. Dozov, M. Nobil, and G. Durand, *Appl. Phys. Lett.* **70**1179 (1997).
16. M. R. Swift, E. Orlandini, W. R. Osborn, and J. M. Yeomans, *Phys. Rev. E* **54**:5041 (1996).